Analytical Model of I–V Characteristics of Arbitrarily Shallow p-n Junctions

Miloš Popadić, Gianpaolo Lorito, and Lis K. Nanver, *Member, IEEE*

***Abstract*—For the first time, an analytical model of arbitrarily shallow p-n junctions is presented. Depending on the junction depth, electrical characteristics of ultrashallow p-n junctions can vary from the characteristics of standard Schottky diodes to standard deep p-n junctions. This model successfully unifies the standard Schottky and p-n diode expressions. In the crossover region, where the shallow doping region can be totally depleted, electrical characteristics phenomenologically substantially different from typical diode characteristics are predicted. These predictions and the accuracy of the presented model are evaluated by comparison with the MEDICI simulations. Furthermore, ultrashallow n^+-p diodes were fabricated, and the anomalous behavior in the crossover regime was experimentally observed.**

***Index Terms*—Schottky barriers, Schottky diodes, semiconductor device modeling, semiconductor diodes, semiconductor junctions.**

I. Introduction

IN THE EVER downscaling of silicon technology, ultrashallow junctions and Schottky diodes are playing an important role as basic building blocks of CMOS transistors [1]. The electrical behavior of such devices can, to a great extent, be simulated by physics-based simulators [2]–[4], but, for many evaluations, compact and efficient analytical models are the more time- and cost-efficient solution [5]. In addition, compact models in simulators extend the complexity of the circuit or device that can be solved. Basic physical principles upon which p-n and Schottky junctions operate have long since been established, and the operation of devices has been well described [6], [7], except for the Schottky barrier height pinning which admittedly remains an issue of debate [8] but is not essential for device modeling. Ultrashallow junctions, however, notwithstanding the attention they receive experimentally [9], [10], have only been given direct theoretical consideration in very few publications [11], [12].

This paper presents a novel analytical model that, for the first time, makes it possible to calculate the I–V characteristics of arbitrarily thin p-n junctions with a metal contact. The model covers the transition of the structure from a Schottky diode (zero junction thickness), over a punchthrough diode (the junction region to the metal can be depleted), to a conventional deep p-n diode. The model successfully calculates punchthrough in the reverse characteristics, and very interestingly, in the forward region new effects related to the depletion of the junction surface from the metal contact are identified. These effects can lead to forward I–V characteristics that significantly differ from the conventional diode behavior with ideality factor $n = 1$. The results are verified by MEDICI simulations, and the novel forward current behavior is also observed experimentally.

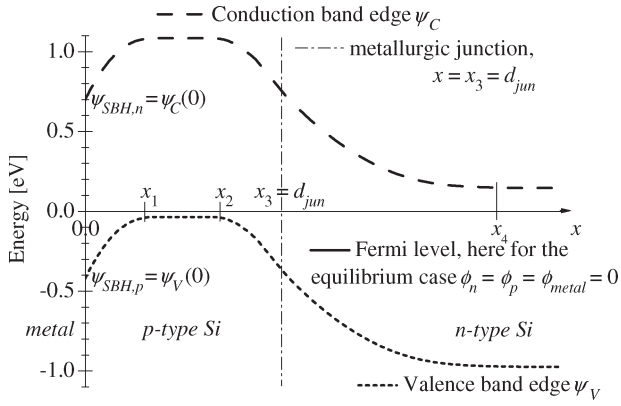

Fig. 1. Schematic band diagram of the structure under consideration. The x-axis is perpendicular to the metal–semiconductor interface and is placed to have this interface at $x = 0$. Planes x_1, x_2, x_3, and x_4 mark the edge of the Schottky depletion region, the edge of the p-n depletion region next to the p-type QNR, the metallurgic p-n junction, and the edge of the p-n junction depletion region next to the n-type QNR, respectively. The vertical axis has zero at the metal Fermi level and is used for both electrons and holes (i.e., for both the conduction and the valence band edge).

This paper is organized as follows. Section II presents the novel unified model for arbitrarily shallow p-n junctions, Section III compares the presented model with the existing Schottky and p-n junction diode characteristics, Section IV compares the predictions of the model in the Schottky/p-n junction transition region with the MEDICI simulations, and Section V presents the measurement results of the fabricated devices which exhibit behavior characteristic of the Schottky to p-n junction transition. Appendices A and B contain details of the model derivation.

II. Analytical Transport Model

We have established an analytical model for carrier transport in a metal/p-Si/n-Si stack as shown in Fig. 1. The p-region may be arbitrarily thick or shallow and forms a Schottky contact to the metal. Of course, the solution for a metal/n-Si/p-Si would be exactly analogous, and therefore, without the loss of generality, we will focus only on the formerly mentioned structure.

Manuscript received May 20, 2008; revised September 4, 2008. Current version published December 19, 2008. The review of this paper was arranged by Editor V. R. Rao.

The authors are with the Delft Institute of Microsystems and Nanoelectronics, Delft University of Technology, 2628 CT Delft, The Netherlands (e-mail: m.popadic@dimes.tudelft.nl).

Digital Object Identifier 10.1109/TED.2008.2009028

The model has been derived by applying the following assumptions: uniform doping profiles with an abrupt transition, the depletion-region approximation, the low-injection regime, constant mobility and lifetimes within each doping region for each carrier type, direct recombination in the quasi-neutral region (QNR), negligible recombination in the depletion region, a finite surface recombination velocity, a constant Schottky barrier height, no tunneling currents, a Maxwellian carrier distribution, and the quasi-Fermi level (QFL) approximation. These approximations are typical of analytical derivations, and their validity will be discussed in more detail hereinafter. The assumption of a flat QFL across the depletion regions, which is also typical for this type of analysis, cannot be justified in situations where the p-region is totally depleted and was therefore not made. Instead, drift and diffusion across depletion regions for both types of carriers were assumed.

The combination of the depletion-region approximation and the low-injection regime assumption means that two kinds of regions may be distinguished. The one is the depletion regions (or space-charge regions) where the concentration of both kinds of free carriers has a negligible impact on the band diagram with respect to the doping, but the carrier concentrations in themselves are not negligible and are considered with respect to charge transport. The other is the QNRs, where the concentration of majority carriers is equal to the doping and the drift current of the majority carriers creates a negligible voltage drop. These two approximations, however, do not prevent the concentration of minority carriers from exceeding the concentration of majority carriers inside the depletion regions.

The derivation begins with the transport equations for both types of carriers: thermionic emission at the metal/Si interface, minority carrier diffusion, and recombination in the QNRs and also drift and diffusion across the depletion regions. The main peculiarity of the problem is that the p-region, if it is thin enough, may be totally depleted. Therefore, reaching the solution depends on both solving the Poisson equation to obtain the band diagram and on solving the transport equations by demanding current and QFL continuity. Formally speaking, these two steps are interlinked and should be solved by a self-consistent iterative algorithm. However, we have shown that it is possible to first assume that the band diagram is known and solve the transport equations as outlined in Appendix A. From that solution, it can be shown that the complete and exact form of the band diagram is not necessary, and the problem can be solved by several mathematically simple and accurate approximations, leaving only the highest potential in the p-region and the p-type QNR width to be calculated as specified in Appendix B. Thereby, we obtain a closed-form solution for the J–V characteristic as a function of the p-region thickness and doping levels.

In the following, the J–V characteristic, as derived in Appendices A and B, is discussed in detail. The current density J, which is the current density across the Schottky junction J^{Sch} and across the p-n junction $J^{\mathrm{p-n}}$, is a sum of the individual electron components, J_n^{Sch} and $J_n^{\mathrm{p-n}}$, and hole components, J_p^{Sch} and $J_p^{\mathrm{p-n}}$

$$J = J^{\mathrm{Sch}} = J^{\mathrm{p-n}} = J_n^{\mathrm{Sch}} + J_p^{\mathrm{Sch}} = J_n^{\mathrm{p-n}} + J_p^{\mathrm{p-n}}. \quad (1)$$

The electron current density component at the p-n junction depletion region is

$$J_n^{\mathrm{p-n}} = qN_C \exp\left(-\frac{\psi_{\mathrm{MB}}}{V_t}\right)\left\langle v_n^{\mathrm{p-n}}\right\rangle\left[\exp\left(\frac{V_a}{V_t}\right) - 1 + G\right] - qn_{p0}G\left\langle v_n^{\mathrm{p-n}}\right\rangle \quad (2)$$

where

$$G = \frac{v_{\mathrm{SchDR},n}^{-1} + \exp\left(\frac{\psi_{\mathrm{SBH},n}-\psi_{\mathrm{MB}}}{V_t}\right)v_{r,n}^{-1} + \frac{E-1}{E+1}v_{D,n}^{-1}}{v_{\mathrm{SchDR},n}^{-1} + \exp\left(\frac{\psi_{\mathrm{SBH},n}-\psi_{\mathrm{MB}}}{V_t}\right)v_{r,n}^{-1} + \frac{E^2+1}{E^2-1}v_{D,n}^{-1}}$$

and where $\langle v_n^{\mathrm{p-n}}\rangle^{-1} = v_{p-\mathrm{nDR},n}^{-1} + (E-1/E+1)v_{D,n}^{-1} + (2EG/E^2-1)v_{D,n}^{-1}$ is an effective electron velocity for the complete structure, as shown from the p-n depletion region, with weighted contributions from $v_{D,n}$, $v_{r,n}$, $v_{\mathrm{SchDR},n}$, and $v_{\mathrm{p-nDR},n}$ which are diffusion velocity, recombination velocity, and effective velocities for crossing the Schottky and p-n junction depletion regions under drift and diffusion for electrons, respectively (see Appendices A and B). The notion of effective velocities is introduced to facilitate the physical phenomenological interpretation of the results. The equilibrium electron concentration in the p-type QNR is n_{p0}, $E = \exp(L_p^{\mathrm{intr}}/L_{D,n})$ is a factor accounting for the thickness of the intrinsic p-region L_p^{intr}, where $L_{D,n}$ is the diffusion length for electrons in the p-region, $\psi_{\mathrm{SBH},n}$ is the Schottky barrier height, ψ_{MB} is the highest value of the bottom of the conduction band in the p-region, q is the elementary charge, N_C is the density of states in the conduction band, $V_t = kT/q$ is the thermal voltage with k as Boltzmann's constant and T as temperature, and V_a is the applied dc voltage. Formulas for obtaining all band-diagram-dependent parameters such as ψ_{MB} and E and, consequently, G and $\langle v_n^{\mathrm{p-n}}\rangle$ are elaborated in Appendix B.

The electron current density component at the Schottky junction depletion region is

$$J_n^{\mathrm{Sch}} = qN_C \exp\left(-\frac{\psi_{\mathrm{MB}}}{V_t}\right)\left\langle v_n^{\mathrm{Sch}}\right\rangle\left[\exp\left(\frac{V_a}{V_t}\right) - H\right] + qn_{p0}(H-1)\left\langle v_n^{\mathrm{Sch}}\right\rangle \quad (3)$$

where

$$H = \frac{E^2-1}{2E}\frac{v_{D,n}}{v_{\mathrm{p-nDR},n}} + \frac{E^2+1}{2E}$$

and where $\langle v_n^{\mathrm{Sch}}\rangle^{-1} = Hv_{\mathrm{SchDR},n}^{-1} + H\exp(-(\psi_{\mathrm{MB}} - \psi_{\mathrm{SBH},n}/V_t))v_{r,n}^{-1} + (H-(1/E))v_{D,n}^{-1} + (1/E)v_{\mathrm{p-nDR},n}^{-1}$ is an effective electron velocity for the complete structure as shown from the Schottky depletion region.

The difference between electron current densities is due to recombination in the quasi-neutral p-region. Therefore, the

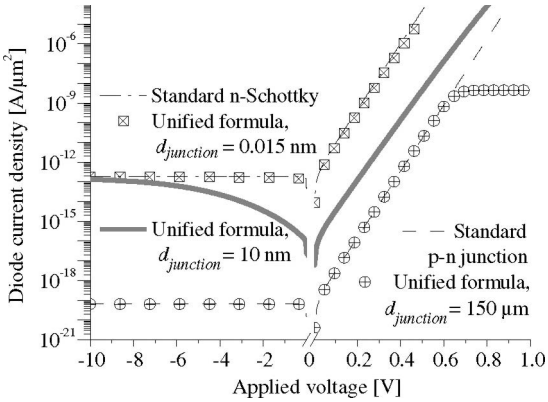

Fig. 2. Current densities of p-n junctions with varying junction depth ($d_{\rm jun}$). Doping levels $N_D = 10^{17}$ cm^{-3} and $N_A = 5 \cdot 10^{18}$ cm^{-3} were assumed in all cases.

limit of $J_n^{\rm Sch}$ as $L_p^{\rm intr}$ approaches zero is $J_n^{\rm p-n}$. Hole current densities, expressed as a function of this difference, are

$$J_p^{\rm p-n} = qp_{n0}\langle v_p\rangle \left[\exp\left(\frac{V_a}{V_t}\right)-1\right] - \frac{J_n^{\rm p-n}-J_n^{\rm Sch}}{\exp\left[(E_g/q-V_n-V_a-\psi_{{\rm SBH},p})/V_t\right]}\cdot\frac{\langle v_p\rangle}{\langle v_n^{\rm diff}\rangle} \quad (4)$$

$$J_p^{\rm Sch} = qp_{n0}\langle v_p\rangle \left[\exp\left(\frac{V_a}{V_t}\right)-1\right] + \left(J_n^{\rm p-n}-J_n^{\rm Sch}\right)\frac{\langle v_p\rangle}{\langle v_n^{\rm diff}\rangle} \quad (5)$$

where the effective velocities are

$$\langle v_n^{\rm diff}\rangle^{-1} = v_{r,p}^{-1} + v_{{\rm SchDR},p}^{-1}$$

$$\langle v_p\rangle^{-1} = v_{{\rm p-nDR},p}^{-1} + v_{D,p}^{-1} + \exp\left[-(E_g/q - V_n - V_a - \psi_{{\rm SBH},p})/V_t\right]\cdot\left(v_{r,p}^{-1} + v_{{\rm SchDR},p}^{-1}\right)$$

where $v_{D,p}$, $v_{r,p}$, $v_{{\rm SchDR},p}$, and $v_{{\rm p-nDR},p}$ are diffusion velocity, recombination velocity, and effective velocities for crossing the Schottky and p-n junction depletion regions under drift and diffusion for holes, respectively, p_{n0} is the equilibrium hole concentration in the n-type QNR, $\psi_{{\rm SBH},p}$ is the Schottky barrier height for holes as shown in Fig. 1, E_g is the Si bandgap, and V_n is the difference in potential between the electron Fermi level and the bottom of the conduction band in the n-type QNR.

III. Transition From p-n Junction to Schottky on n-Si

Equations (1)–(5) represent a closed-form unified solution covering the whole spectrum of junction configurations from a Schottky contact on n-Si to a conventional deep p-n junction. Indeed, it can be shown analytically that the unified expression approaches standard Schottky diode and p-n diode expressions as the junction depth approaches zero and infinity, respectively. In Fig. 2, an example of the evolution of J–V characteristics as a function of the junction depth is presented for a particular arbitrarily chosen structure with the doping levels of $N_A = 5 \cdot 10^{18}$ cm^{-3} and $N_D = 10^{17}$ cm^{-3}. It is evident that

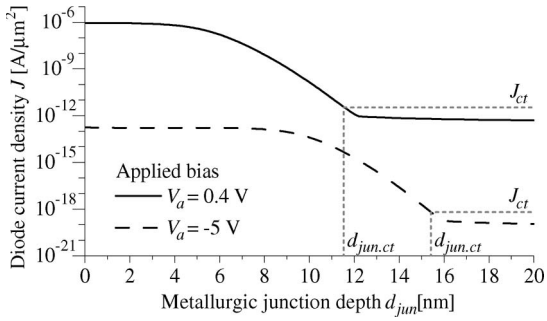

Fig. 3. Current densities as a function of p-region width at fixed bias points, according to the analytical model for a device with $N_D = 10^{17}$ cm^{-3} and $N_A = 5 \cdot 10^{18}$ cm^{-3}. The dotted line marks the nonphysical critical point defined by $J(d_{\rm jun} = d_{\rm jun.ct}) = J_{\rm ct} = 10 \cdot J(d_{\rm jun} = 1\ \mu{\rm m})$.

the unified expression for the current (1) for the limit of $d_{\rm jun} \to 0$ yields the standard Schottky expression [7], whereas the limit of $d_{\rm jun} \to \infty$ yields the standard p-n junction expression [7]. In Fig. 2, this is shown by using unrealistically extreme values of junction depth; however, it can also be shown analytically, e.g., for the limit of $d_{\rm jun} \to 0$, we have $E \to 1$, $G \to 0$, $H \to 1$, and $\lim_{d_{\rm jun}\to 0}\langle v_n^{\rm p-n}\rangle^{-1} = \lim_{d_{\rm jun}\to 0}\langle v_n^{\rm Sch}\rangle^{-1} = v_{\rm p-nDR,n}^{-1} + v_{\rm SchDR,n}^{-1} + \exp(\psi_{{\rm SBH},n} - \psi_{\rm MB}/V_t)v_{r,n}^{-1} \approx v_{r,n}^{-1}$ as $\psi_{\rm MB} = \psi_{{\rm SBH},n}$, which reduces both (2) and (3) to the same standard expression for the current of a Schottky junction. The hole current in this Schottky-diode case is negligible compared to the electron current. Similarly, the limit of $d_{\rm jun} \to \infty$ can be easily calculated.

In addition, it can be seen from Fig. 2 that the characteristic in the transition region is phenomenologically different from both extremes, exhibiting nonideal behavior in both the forward (here, the ideality factor is $n \approx 1.1$) and the reverse regime. Another example of the current level transition from the Schottky ($d_{\rm jun} = 0$) to the p-n junction current levels ($d_{\rm jun} = 20$ nm) is shown in Fig. 3 as a continuous function of the junction depth. This characteristic is not universal, but instead, the transition-region position depends on the biasing voltage and on the doping levels (here, $N_D = 10^{17}$ cm^{-3} and $N_A = 5 \cdot 10^{18}$ cm^{-3}). To illustrate this, we define the critical junction depth as the junction depth at which the current at a certain applied voltage is exactly one order of magnitude higher than the current of the diode with a junction depth of $d_{\rm jun} = 1\ \mu$m. This definition does not infer any physical significance but is only chosen such that, in the majority of cases, it corresponds to the onset of the total p^+ region depletion. A plot of the thus defined critical junction depth as a function of p^+ doping for different n-doping and applied voltage combinations is shown in Fig. 4. Therefore, the hereby presented model can be used both to predict ultrashallow junction behavior (as in Fig. 2) and to predict when a device will start exhibiting behavior substantially different from conventional deep p-n diodes (as in Fig. 4).

IV. I–V Characteristics: Verification by Simulation and Discussion

We have employed a MEDICI device simulator to evaluate the accuracy of the analytically derived dependencies, and

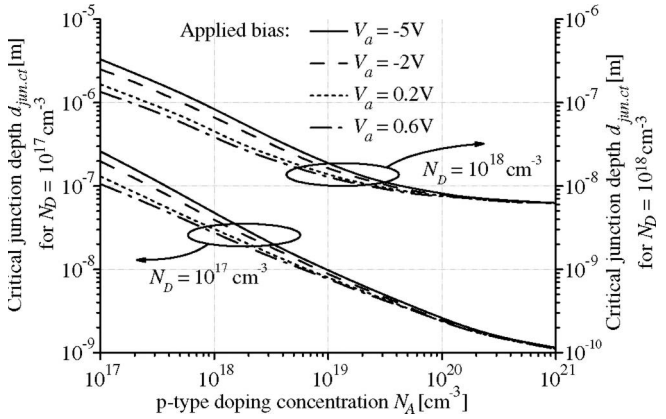

Fig. 4. Critical junction depth as a function of p^+ doping for different n-doping and applied voltage combinations. Critical junction depth is defined as a junction depth at which the current is ten times the current of an otherwise identical structure with $d_{\rm jun} = 1$ μm.

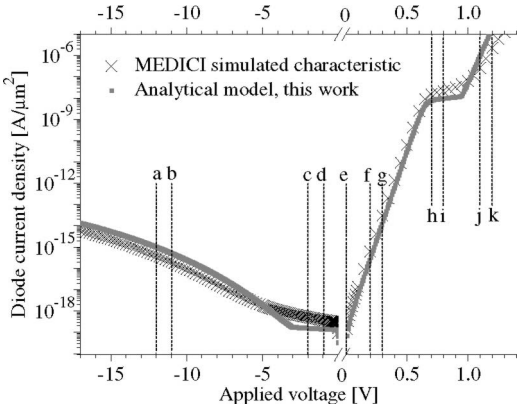

Fig. 5. Comparison between the metal-p-n diode current densities obtained from the analytical model presented here (1) and from the MEDICI simulation of the same structure ($d_{\rm jun} = 15$ nm, $N_D = 10^{17}$ cm^{-3}, $N_A = 5 \cdot 10^{18}$ cm^{-3}, and SBH$_p = 0.42$ V). No fitting parameters were used.

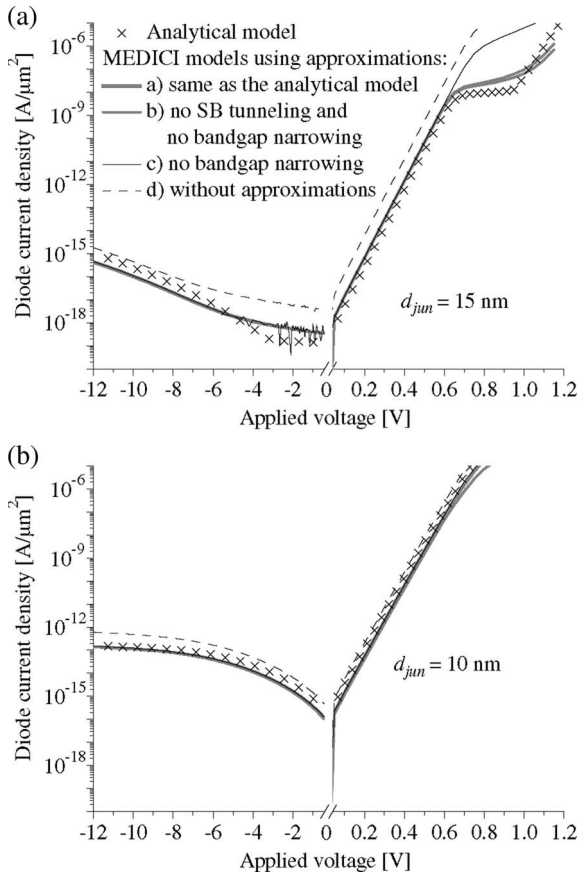

Fig. 6. Comparison of MEDICI-simulated characteristics under different approximations. A bias-depleted device (BDD) with $d_{\rm jun} = 15$ nm is considered in plot (a), and a fully depleted device (FDD) with $d_{\rm jun} = 10$ nm is considered in plot (b).

an arbitrarily chosen exemplary comparison is shown in Fig. 5. As in Figs. 2 and 3, a device with $N_A = 5 \cdot 10^{18}$ cm^{-3}, $N_D = 10^{17}$ cm^{-3}, and SBH for holes of 0.42 V was considered. The junction depth at $d_{\rm jun} = 15$ nm was deliberately chosen close to the point at which the p-region only becomes totally depleted. In this manner, the ability of the analytical model to predict all the different modes of operation can be tested. In Fig. 5, the same constant values for carrier mobility, surface recombination velocity, carrier lifetimes, and SBH were set in the 1-D MEDICI simulation and in the analytical model, but no fitting parameters were used to improve the fit. The remaining small discrepancies between the simulation results and the analytical model are due to the fact that the simulation implements a smooth transition between the depletion regions and QNRs, recombination in the depletion regions, and serial resistances of the QNRs, unlike the analytical model. Corresponding band diagrams obtained from the MEDICI simulation at the specified points are shown in Fig. 7.

In Fig. 6, the results of different MEDICI-simulated characteristics, with and without approximations, are compared with each other and with the analytical model. This was done for two devices, with junction depths of 10 nm and 15 nm using different approximations: a) A MEDICI model as similar as possible to the analytical model was used without Fermi–Dirac statistics (FDS), Auger recombination (AR), Schottky barrier tunneling (SBT), or bandgap narrowing (BGN); b) FDS and AR have been included but not SBT and BGN; c) only the BGN is not included; and d) none of the mentioned approximations were made. It can be seen that the inclusion of FDS and AR [difference between a) and b)] makes a completely negligible difference, too small to be seen in this figure; the inclusion of SBT [difference between c) and b)] has an influence only in the far-forward regime, and it is plausible that it can, to a good extent, be approximated in the analytical model with an effectively lower SBH; and the BGN [difference between d) and c)] creates a significant increase in the current levels, which can be easily included in the analytical model. The presented simulation, however, did not consider the fabrication-dependent Shockley–Read–Hall recombination on defects, which can, in many applications, be a factor that significantly affects device behavior. Good analytical models of SBH tunneling and recombination exist [13] and can be integrated with this model. Another possible improvement can be achieved by more realistic modeling of the depletion region to QNR transition [14], which would slightly improve the accuracy of the effective velocities for crossing the depletion region (see Appendix B). For that purpose, also a more elaborate mobility model can be used [15]. It remains, however, questionable which of these

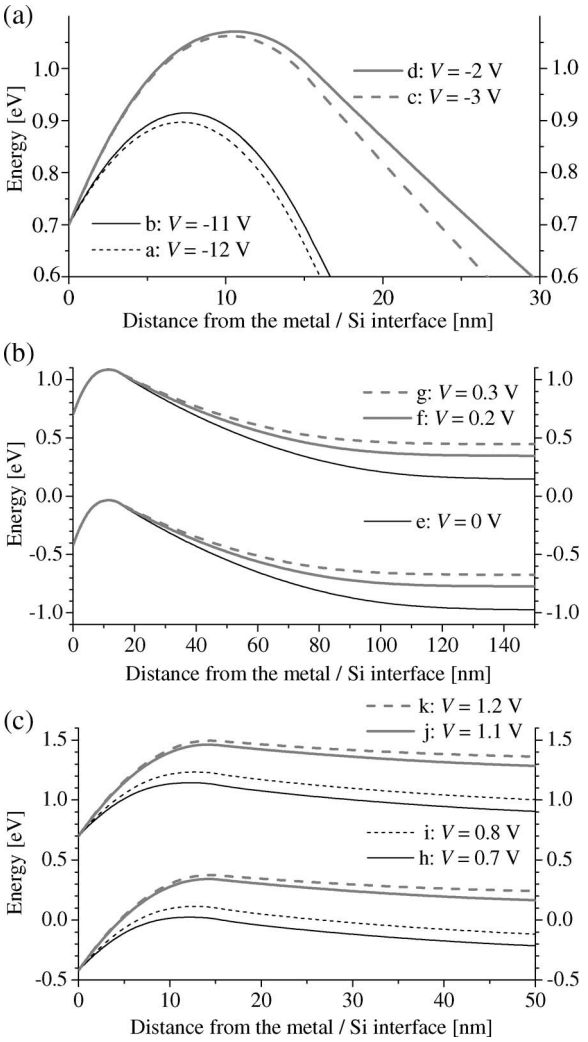

Fig. 7. Conduction- and valence-band edges obtained from the MEDICI simulation for different biasing of the structure considered in Fig. 4. Energy is measured from the metal Fermi level. In plot (a), only the conduction band edges under reverse biasing are presented; (b) plots the band diagram in case of moderate forward biasing; and (c) represents the case of strong forward bias.

extensions of the model can be made while still keeping the end result in a closed form (i.e., without having to introduce an iterative algorithm). However, even with no improvements made, Fig. 6 shows that the present analytical model gives a good prediction of the real device behavior, particularly in the case of the fully depleted device (with a junction depth of 10 nm), which is a transition characteristic of our primary interest.

The characteristic shown in Fig. 5, predicted by our analytical model and the MEDICI simulation, is another example of a J–V characteristic in the transition region between Schottky on n-Si to deep p-n junction characteristics exhibiting a behavior very different from a standard diode characteristic, as a consequence of an exceptionally shallow junction depth. This behavior can be explained by considering Fig. 7 that shows a series of band diagrams, obtained from the MEDICI device simulator, calculated at the biasing points specified in Fig. 5.

It was already pointed out that the J–V characteristics of ultrashallow devices described here are strikingly different from standard p-n junctions or Schottky diodes. This difference originates from the thin p-region that can either be totally depleted even without any bias applied [fully depleted device (FDD)] or can become depleted under bias [bias-depleted device (BDD)]. The characteristics of FDDs and BDDs are also very different as can be seen by comparing Fig. 6(a) where an example of a BDD is featured and Fig. 6(b) that represents a FDD. Under reverse bias of a BDD, at a certain point, an increase in the reverse saturation current can appear (Fig. 5) due to a reduction of the highest band potential when the p-region is totally depleted [Fig. 7(a), difference between band diagrams a and b]. Such a potential barrier decrease exists already at the beginning of the reverse characteristic in case of a FDD (Fig. 2), but not in case of a BDD before the p-region becomes depleted [Fig. 7(a), difference between band diagrams c and d]. The increase in both cases saturates at the reverse current level of the p-Schottky (Fig. 2, direct example and Fig. 3, indirect example), as the highest band potential in the p-region cannot fall under the value of the SBH for holes. In the forward regime, the current initially increases exponentially in case of a BDD [Fig. 5 and corresponding Fig. 7(b)], and the device differs from the wide p-n junction only because the diffusion of electrons in the p-region is not determined by their diffusion length but by the thickness of the p-QNR which is much smaller. However, in case of a FDD, the highest band potential in the p-region will increase with the biasing, and the forward characteristic will be nonideal (Fig. 2). In the far-forward regime of a BDD, a current saturation can appear (Fig. 5) when the reverse-biased p-Schottky contact cannot support further increase in the hole current across the p-n junction [Fig. 7(c), i and h]. Increasing the applied voltage further biases the p-Schottky contact in reverse, and the current starts to increase again when the p-type QNR becomes totally consumed by the increasing p-Schottky depletion region [Fig. 7(c), j and k]: The increase in the maximum potential inside the p-region is much smaller than the bias increase, which leads to an increase in the electron current from Si to the metal, and the device then essentially behaves like an n-Schottky diode, or as a FDD in the forward regime.

V. Experimental Observation of Ultrashallow Behavior

The anomalous I–V characteristics were also observed in specially fabricated ultrashallow n^+p diodes. Layers of As and P were first deposited by chemical vapor deposition and consequently annealed for 20 min at different temperatures. The thermal step causes diffusion from deposited layers of As or P [16], forming junctions with junction depths from less than 5 nm to around 15 nm [17].

Effects predicted by the model presented here have been measured, and examples are shown in Fig. 8. Depending on the amount of diffused n-type doping, on the reverse characteristics, either a sudden onset of a gradual current increase [point marked by (3)] at the onset of total depletion of the n^+ region, as in Fig. 5, or a continuous increase saturating at the expected ideal Schottky diode current level, as in Fig. 2, is evident. This is due to the biasing that reduces the effective barrier height, and this trend continues until the onset of breakdown [point marked by (4)]. This should not be confused with the increase

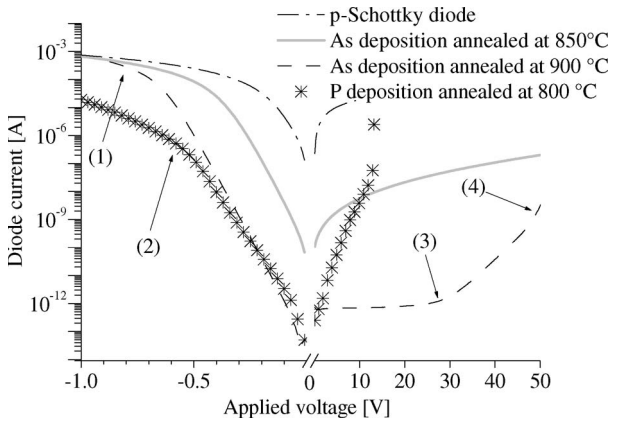

Fig. 8. Measured diode I–V characteristics of ultrashallow n^+p diodes. The diodes have n^+ regions that are diffused from little more than 0 to about 15 nm into the Si surface, and they are doped up to $5 \cdot 10^{19}$ cm^{-3} against the background of 10^{17} cm^{-3}.

in the reverse current due to leakage that can be seen on the characteristic of the sample with the annealed P layer.

On the forward characteristics, the more lightly doped samples show that at the point marked by (2), the reverse-biased n-Schottky contact starts limiting the total current before the series resistance does [point marked by (1)], as in Fig. 5. These effects have also been discussed in relation to Fig. 5 and the band diagrams presented in Fig. 7.

Fig. 8 enables only a qualitative discussion; for an exact quantitative comparison of the model predictions with the measurements, the doping profiles of the fabricated devices would have to be known, which was impossible to obtain due to a combination of shallowness and a large amount of surface deposited As that has not diffused.

VI. Conclusion

We developed, for the first time, an analytical closed-form model for arbitrarily shallow metal-contacted p-n junctions. It has been demonstrated that the model accurately predicts the I–V characteristics of depletable junctions covering the whole spectrum from Schottky to p-n junctions and can be used both to predict the behavior of an ultrashallow junction and to predict the onset of total depletion in the ultrashallow junction. The solution that we present can be very attractive for new device compact models.

The accuracy of the model is limited by the validity of approximations under which it has been derived. We have shown that among them, tunneling through the Schottky barrier and BGN are most likely to significantly affect the diode characteristics in certain modes of operations. We believe that the latter can be easily incorporated into the model, whereas the former can be partly accounted for by using a lower effective Schottky barrier height value in the model. This also means that integrating this model with one of the existing analytical diode models that include tunneling would be very attractive.

The model also reveals previously unrecognized phenomena in the transition region between an n-Schottky diode and a deep p-n junction. These effects may lead to ideality factors significantly higher than $n = 1$. Since extremely shallow junctions are used in, for example, advanced CMOS transistors, this type of analytical model can play an important role in identifying the source of nonidealities and for describing the general device behavior.

Appendix A

In this Appendix, the outline of the derivation of (2)–(5) is presented. These equations combined, form the final J–V characteristic given by (1) for a metal/p-Si/n-Si stack where the p-region may be arbitrarily shallow and forms a Schottky contact to the metal. The band diagram of the structure is schematically shown in Fig. 1, together with the axes that will be used in the derivation. On the spatial axis x, points $x = 0$, x_1, x_2, x_3, and x_4, respectively, mark the following interface planes: metal-to-semiconductor interface, Schottky depletion region to p-type QNR interface, p-type QNR to p-n depletion-region interface, and p-n depletion region to n-type QNR interface. In case of a totally depleted p-region, we will set $x_1 = x_2 = x_{\mathrm{MB}}$, where x_{MB} is the x-coordinate of the highest potential in the p-region. The energy axis is positioned to have a zero at the metal Fermi level.

A. Transport Mechanisms

We begin by considering the transport mechanisms in different regions of the structure. At the metal-to-semiconductor interface, the thermionic emission current density for electrons and holes $J^M_{\langle n|p\rangle}$ is given by [7]

$$J^M_{\langle n|p\rangle} = qv_{r,\langle n|p\rangle}\left(\langle n|p\rangle^{\mathrm{DR}}(0) - \langle n|p\rangle_0^{\mathrm{DR}}\right) \tag{6}$$

where $\langle n|p\rangle$ is a compact notation allowing formulas for electrons and holes to be written together, i.e., it should be read as two independent formulas where the symbol $\langle n|p\rangle$ is in the first formula substituted with n and in the second with p. As an index, it denotes a physical property of electrons or holes, and as a stand-alone symbol, it denotes electron and hole concentrations, in (6) specifically $n^{\mathrm{DR}}(0)$ and $p^{\mathrm{DR}}(0)$ as electron and hole concentrations in the depletion region at the metal–semiconductor interface (coordinate $x = 0$), and n_0^{DR} and p_0^{DR} as equilibrium (without any voltage applied) concentrations. Furthermore, $v_{r,\langle n|p\rangle} = \sqrt{kT/2m^*_{\langle n|p\rangle}\pi}$ is the recombination velocity at the metal–semiconductor interface, with k equal to Boltzmann's constant, T as the absolute temperature, and m^* as the effective mass. Of course, in a specific case, a surface recombination velocity different from that theoretically predicted can be used.

In both Schottky and p-n depletion regions, the current of both types of carriers $J^{\mathrm{DR}}_{\langle n|p\rangle}(x)$ is given by drift and diffusion, represented together by using the gradient of the QFL $\phi_{\langle n|p\rangle}(x)$

$$J^{\mathrm{DR}}_{\langle n|p\rangle}(x) = \langle n|p\rangle^{\mathrm{DR}}(x)\mu_{\langle n|p\rangle}\frac{d\phi_{\langle n|p\rangle}(x)}{dx} \tag{7}$$

where $\mu_{\langle n|p\rangle}$ is the electron/hole mobility.

Finally, in the QNRs, we assume a negligible electric field and voltage drop implying a constant QFL for majority carriers.

Therefore, the minority carriers move only by diffusion and are under direct recombination given by

$$U_{\langle p|n\rangle} = \frac{\langle p|n\rangle_{\langle n|p\rangle} - \langle p|n\rangle_{\langle n|p\rangle,0}}{\tau_{\langle p|n\rangle}} \tag{8}$$

where $\tau_{\langle p|n\rangle}$ are carrier lifetimes, p_n and n_p are minority carrier concentrations (hole concentration in n-type Si and electron concentration in p-type Si), and $\langle p|n\rangle_{\langle n|p\rangle,0} = n_i^2/\langle N_D|N_A\rangle$ are equilibrium concentrations.

Therefore, in the QNR, the continuity equation for minority carriers

$$\frac{\partial\langle n|p\rangle}{\partial t} = \frac{1}{q}\nabla J_{\langle n|p\rangle} - U_{\langle n|p\rangle} = 0 \tag{9}$$

where $U_{\langle n|p\rangle}$ are the recombination-generation rates, together with the diffusion current

$$J_{\langle n|p\rangle} = \langle +|-\rangle D_{\langle n|p\rangle} q \frac{d\langle n|p\rangle}{dx} \tag{10}$$

where $D_{\langle n|p\rangle}$ are the diffusion constants, and the assumption made that the n-type QNR is much larger than the diffusion length $L_{D,p}$ yields

$$p_n = \Delta p_n \exp\left(-\frac{x}{L_{D,p}}\right) + p_{n,0}. \tag{11}$$

In the case of the finite p-region, this yields

$$n_p = \Delta n_1 \exp\left(\frac{x}{L_{D,n}}\right) - \Delta n_2 \exp\left(-\frac{x}{L_{D,n}}\right) + n_{p,0}. \tag{12}$$

B. Current Density—QFL Relations

In this section, we first express the current densities as a function of QFLs for distinct parts of the structure. It should be noted that for simplicity in the course of derivation in this appendix, the band edges (ψ) and QFLs (ϕ) are regarded as energy, not voltage, and are measured from the metal Fermi level, with one energy axis for both electrons and holes, meaning that the valence band edge would normally have a negative energy value if no voltage is applied as shown in Fig. 1. Therefore, electron and hole concentrations can always be represented as

$$\langle p|n\rangle = \langle N_V|N_C\rangle \mathrm{e}^{\langle +|-\rangle \frac{\psi_{\langle V|C\rangle} - \phi_{\langle p|n\rangle}}{kT}}. \tag{13}$$

However, in (1)–(5) they are converted back to voltage, which is a more common representation.

The hole diffusion current in the n-type QNR (i.e., for $x > x_4$, superscript index Nqnr), is from (11)

$$J_p^{\mathrm{Nqnr}} = \frac{q v_{D,p} n_i^2}{N_D}\left[\exp\left(\frac{qV_a}{kT} - \frac{\phi_p(x_4)}{kT}\right) - 1\right] \tag{14}$$

where $v_{D,\langle n|p\rangle} \triangleq (D_{\langle n|p\rangle}/L_{D,\langle n|p\rangle})$ are the diffusion velocities, n_i is the intrinsic concentration, and V_a is the applied dc bias.

The hole drift and diffusion current in the p-n depletion region (i.e., for $x_2 < x < x_4$, superscript index p-n) is from (7), after integration over x_2 to x_4

$$J_p^{\mathrm{p-n}} I_{V24} = N_V kT\mu_p\left[\exp\left(-\frac{\phi_p(x_2)}{kT}\right) - \exp\left(-\frac{\phi_p(x_4)}{kT}\right)\right] \tag{15}$$

where we define

$$I_{V24} \triangleq \int_{x_2}^{x_4} \exp\left(-\frac{\psi_V(x)}{kT}\right) dx \tag{16}$$

with ψ_V equal to the top of the valence band and N_V denoting density of states in the valence band.

The same is valid for electrons in the p-n depletion region

$$J_n^{\mathrm{p-n}} I_{C24} = N_C kT\mu_n\left[\exp\left(\frac{qV_a}{kT}\right) - \exp\left(\frac{\phi_n(x_2)}{kT}\right)\right] \tag{17}$$

where

$$I_{C24} \triangleq \int_{x_2}^{x_4} \exp\left(\frac{\psi_C(x)}{kT}\right) dx \tag{18}$$

where ψ_C is the bottom of the conduction band.

In the p-type QNR (i.e., $x_1 < x < x_2$, superscript index Pqnr), the concentration of holes is N_A, and the concentration of electrons is given by

$$n^{\mathrm{Pqnr}}(x) = N_C \exp\left(-\frac{\psi_C(x_1) - \phi_n(x)}{kT}\right) = \frac{n_i^2}{N_A} + \Delta n(x) \tag{19}$$

where from (12)

$$\Delta n(x) = \Delta n_1 \exp\left(\frac{x - x_1}{L_{D,n}}\right) - \Delta n_2 \exp\left(-\frac{x - x_1}{L_{D,n}}\right). \tag{20}$$

Since the electron current in the p-type QNR is diffusion current ($J_n = D_n q(dn/dx)$), from (20), we have

$$J_n^{\mathrm{Pqnr}}(x_1) = q v_{D,n}(\Delta n_1 + \Delta n_2) \tag{21}$$

$$J_n^{\mathrm{Pqnr}}(x_2) = q v_{D,n}\left(\Delta n_1 E + \frac{\Delta n_2}{E}\right) \tag{22}$$

where we introduce $E \triangleq \exp(x_2 - x_1/L_{D,n})$.

In the Schottky depletion region (i.e., $0 < x < x_1$, superscript index Sch), analogously as in the p-n depletion region, the hole and electron drift and diffusion currents after integration yield

$$J_p^{\mathrm{Sch}} I_{V01} = N_V kT\mu_p\left[\exp\left(-\frac{\phi_p(0)}{kT}\right) - \exp\left(-\frac{\phi_p(x_1)}{kT}\right)\right] \tag{23}$$

$$J_n^{\mathrm{Sch}} I_{C01} = N_C kT\mu_n\left[\exp\left(\frac{\phi_n(x_1)}{kT}\right) - \exp\left(\frac{\phi_n(0)}{kT}\right)\right] \tag{24}$$

with

$$I_{V01} \triangleq \int_0^{x_1} \exp\left(-\frac{\psi_V(x)}{kT}\right) dx \tag{25}$$

$$I_{C01} \triangleq \int_0^{x_1} \exp\left(\frac{\psi_C(x)}{kT}\right) dx. \tag{26}$$

Finally, at the metal–Si interface (i.e., $x \approx 0$, superscript index M), based on (6), we write

$$J_n^M = qv_{r,n}N_C \exp\left(-\frac{\psi_C(0)}{kT}\right)\left[\exp\left(\frac{\phi_n(0)}{kT}\right) - 1\right] \tag{27}$$

$$J_p^M = qv_{r,p}N_V \exp\left(\frac{\psi_V(0)}{kT}\right)\left[1 - \exp\left(-\frac{\phi_p(0)}{kT}\right)\right]. \tag{28}$$

C. Boundary Conditions

The boundary conditions comprise QFL and band edge continuity, which were directly implemented in (14)–(28), and the constant total current. In addition, by neglecting the carrier generation and recombination in all regions, except the QNRs, both electron and hole current components must remain constant in all regions excluding the QNRs.

This means that

$$J_p^{\mathrm{Nqnr}} = J_p^{\mathrm{p-n}} \tag{29}$$

$$J_p^{\mathrm{Sch}} = J_p^M \tag{30}$$

$$J_n^{\mathrm{Pqnr}}(x_1) = J_n^{\mathrm{Sch}} = J_n^M \tag{31}$$

$$J_n^R \triangleq J_n^{\mathrm{Pqnr}}(x_2) = J_n^{\mathrm{p-n}} \tag{32}$$

$$J_n^{\mathrm{Sch}} + J_p^{\mathrm{Sch}} = J_n^{\mathrm{p-n}} + J_p^{\mathrm{p-n}}. \tag{33}$$

D. Linearization and Solution of the Equation Set

In order to solve the set of equations (14)–(33), they are linearized by regarding $\exp(\langle+|-\rangle(\phi_{\langle n|p\rangle}(x)/kT))$ factors at different x positions as unknowns, and it is assumed that the band diagram is known. One compact way toward the solution is outlined in the following.

From (24), (27), and (31), J_n^{Sch} can be expressed as a function of the QFL on the Schottky junction border of p-type QNR ($x = x_1$), and using (17) where $J_n^{\mathrm{p-n}}$ is expressed as a function of the QFL on the p-n junction border of p-type QNR ($x = x_2$), together with (19) and (20), we obtain formulas for $n^{\mathrm{Pqnr}}(x_{\langle 1|2\rangle})$. Combining the former with the latter two and taking advantage of relations (21) and (22) results in two linear equations relating $J_n^{\mathrm{p-n}}$ and J_n^{Sch}, which result in equations given by (2) and (3) after defining effective velocities for crossing Schottky and p-n depletion regions for holes and electrons as

$$v_{\langle \mathrm{Sch}|\mathrm{p-n}\rangle \mathrm{DR},p} \triangleq \frac{D_p}{I_{V\langle 01|24\rangle} \exp\left(+\frac{\min\left(\psi_V\left(x_{\langle 0|2\rangle}\right),\psi_V\left(x_{\langle 1|4\rangle}\right)\right)}{kT}\right)} \tag{34}$$

$$v_{\langle \mathrm{Sch}|\mathrm{p-n}\rangle \mathrm{DR},n} \triangleq \frac{D_n}{I_{C\langle 01|24\rangle} \exp\left(-\frac{\max\left(\psi_C\left(x_{\langle 0|2\rangle}\right),\psi_C\left(x_{\langle 1|4\rangle}\right)\right)}{kT}\right)}. \tag{35}$$

These effective velocities do depend on the band diagram but can be easily and, with very good accuracy, approximately calculated as explained in Appendix B.

The hole current expressions are obtained analogously, first $J_p^{\mathrm{p-n}}$ is expressed as a function of the QFL at the p-n junction border of the p-type QNR, from (14), (15), and (29), and the same is done for J_p^{Sch} from (23), (28), and (30). These two equations combined with the already obtained solutions for the electron current density can be solved to yield the hole current solution presented in (4) and (5).

APPENDIX B

Equations (1)–(5) represent the result for J–V characteristics that contains parameters dependent on the band diagram. In this Appendix, we show how the values of these parameters are calculated.

A. Evaluation of Velocities for Crossing Depletion Regions

Velocities for crossing depletion regions $v_{\mathrm{p-nDR},\langle p|n\rangle}$ and $v_{\mathrm{SchDR},\langle p|n\rangle}$, as defined in (34) and (35), contain in the denominator an integral, whose integrand, at one border of the integration interval (we can assume that this is the beginning of the integration interval), is equal to one and, toward the end of the integration interval, decreases quickly (exponentially or faster) from that value. More specifically, in the case of the Schottky depletion region, if the beginning of the integration interval is at the metal–semiconductor interface, the velocities for crossing this depletion region can be accurately approximated by

$$\begin{aligned} v_{\mathrm{SchDR},\langle n|p\rangle} &= \frac{D_{\langle n|p\rangle}}{\int_0^{x_1} \exp\left(\langle-|+\rangle \frac{\psi_{\mathrm{SBH},\langle n|p\rangle} - \psi_{\langle C|V\rangle}(x)}{kT}\right)} \\ &\cong \frac{D_{\langle n|p\rangle}}{\int_0^{\infty} \exp\left(-\frac{qE_f x}{kT}\right)} \\ &= \frac{D_{\langle n|p\rangle} qE_f}{kT} \\ &= \mu_{\langle n|p\rangle} E_f \end{aligned} \tag{36}$$

where E_f is the electric field at the interface. Of course, in the majority of cases, this electric field will be too high for (36) to be valid, and the real velocity for crossing the Schottky depletion region will be equal to the saturation velocity $v_{\mathrm{sat},\langle n|p\rangle}$. In all other cases, the beginning of the integration interval will be the edge of the depletion region at the interface with the QNR. In the same manner as in (36), we write

$$\begin{aligned} v_{\mathrm{DR},\langle n|p\rangle} &= \frac{D_{\langle n|p\rangle}}{\int_{x_i}^{x_j} \exp\left(\langle-|+\rangle \frac{\psi_{\langle n|p\rangle}(x_i) - \psi_{\langle C|V\rangle}(x)}{kT}\right)} \\ &\cong \frac{D_{\langle n|p\rangle}}{\int_0^{\infty} \exp\left(-\frac{q^2 N_{\langle A|D\rangle} x^2}{\varepsilon kT}\right)} \\ &= 2\sqrt{\frac{kTN_{\langle A|D\rangle}}{\pi\varepsilon}} \mu_{\langle n|p\rangle}. \end{aligned} \tag{37}$$

In special cases, acceptor doping concentration N_A may be relevant for the hole carrier velocity, or donor doping concentration N_D may be relevant for the electron carrier velocity.

B. Band Edges of the Totally Depleted p-Region

If the p-region is totally depleted, the Poisson equation in case of uniform doping, as we have assumed and under the depletion-region approximation, readily results in the following expressions for the position of the point of highest value of the conduction band edge x_{MB} and its value ψ_{MB}, in (38) and (39) shown at the bottom of the page.

Of course, if x_{MB} as obtained from (38) is negative, then the highest value of the conduction band edge is at the metal–semiconductor interface, and $\psi_{\mathrm{MB}} = \psi_{\mathrm{SBH},n}$.

C. Band Edges of the p-QNR

If the p-QNR exists, the Poisson equation alone is not sufficient to solve the band diagram. Instead, the top of the valence band is related to the QFL for holes, whose position is determined according to the analysis presented in Appendix A. Therefore, from (4), where $J_p^{\mathrm{p-n}}$ is expressed as a function of the QFL at the p-n junction border of the p-type QNR, and from (14), (15), and (29), assuming that the p-QNR exists, we obtain

$$qp_{n0}\langle v_p\rangle\left[\exp\left(\frac{V_a}{V_t}\right)-1\right] - \frac{J_n^{\mathrm{p-n}}-J_n^{\mathrm{Sch}}}{\exp\left[(E_g-V_n-V_a-\psi_{\mathrm{SBH},p})/V_t\right]}\cdot\frac{\langle v_p\rangle}{\langle v_n^{\mathrm{diff}}\rangle} = qN_V\frac{\exp\left(\frac{E_g-qV_p-\psi_C(x_1)}{kT}\right)-\exp\left(-\frac{qV_a}{kT}\right)}{\frac{I_{V24}}{D_p}+\frac{\exp\left(-\frac{\psi_V(x_4)+qV_a}{kT}\right)}{v_{D,p}}} \tag{40}$$

where $V_{\langle p|n\rangle} = kT\ln(N_{\langle V|C\rangle}/N_{\langle A|D\rangle})$ is the voltage difference between the Fermi level and the band edge in the QNR. We will use this equation to obtain $\psi_C(x_1)$. If $L_p^{\mathrm{intr}} < x_3 \ll L_{D,n}$, then the difference in electron currents can be neglected, and (40) is simplified to yield

$$\psi_C(x_1) = E_g - qV_p + qV_a - kT\ln\left[\frac{\frac{1}{v_1}+\frac{1}{v_2}\exp\left(\frac{qV_a}{kT}\right)}{\frac{1}{v_1}+\frac{1}{v_2}}\right] \tag{41}$$

where

$$\frac{1}{v_1} = \exp\left(\frac{qV_a+V_n-E_g-\psi_{\mathrm{SBH},p}}{kT}\right)\left(\frac{1}{v_{r,p}}+\frac{1}{v_{\mathrm{SchDR},p}}\right)$$

$$\frac{1}{v_2} = \frac{1}{v_{\mathrm{p-nDR},p}}+\frac{1}{v_{D,p}}.$$

If the junction depth is comparable or larger than the electron diffusion length, the difference in electron currents cannot be neglected. After substitution of (2) and (3) into (40) and a number of transformations, we obtain (42) shown at the bottom of the page.

From (41) and (42), $\psi_C(x_1)$ can be calculated with $v_{\mathrm{SchDR},p}$ approximated as $v_{\mathrm{sat},p}$. Such an approximation will have a negligible impact on the accuracy of $\psi_C(x_1)$. After $\psi_C(x_1)$ is obtained, $v_{\mathrm{SchDR},p}$ can also be calculated based on the Poisson equation and (36) as

$$v_{\mathrm{SchDR},p} = \sqrt{\frac{2N_A\left(\psi_C(x_1)-\psi_{\mathrm{SBH},n}\right)}{\varepsilon}}\mu_p. \tag{43}$$

If, for a particular applied voltage, this value is found to be lower than $v_{\mathrm{sat},p}$, $\psi_C(x_1)$ can easily be recalculated.

If the p-QNR exists, after solving the Poisson equation, knowing $\psi_C(x_1)$, we obtain that the edges of the depletion regions are at

$$x_1 = \sqrt{\frac{2\varepsilon\left(\psi_C(x_1)-\psi_{\mathrm{SBH},n}\right)}{N_Aq^2}} \tag{44}$$

$$x_2 = x_3 - \sqrt{\frac{2\varepsilon N_D\left(\psi_C(x_1)-qV_a-V_n\right)}{N_Aq^2(N_A+N_D)}}. \tag{45}$$

From (44) and (45), E_f is obtained.

$$x_{\mathrm{MB}} = x_3\left(1+\frac{N_D}{N_A}\right)-\sqrt{\left(x_3\frac{N_D}{N_A}\right)^2+\frac{2N_D\varepsilon(\psi_{\mathrm{SBH},n}-qV_a-V_n)}{q^2N_A^2}+\frac{N_D}{N_A}x_3^2} \tag{38}$$

$$\psi_{\mathrm{MB}} = qV_a+V_n+\frac{q^2N_A(x_3-x_{\mathrm{MB}})^2}{2\varepsilon}\left(1+\frac{N_A}{N_D}\right) \tag{39}$$

$$\psi_C(x_1) = -kT\ln\left[\frac{\frac{1}{v_1}\left(1+2\frac{v_{D,n}}{v_{D,p}}\cdot\frac{N_D}{N_A}\cdot\frac{E-1}{E+1}\right)+\frac{1}{v_2}\exp\left(\frac{qV_a}{kT}\right)}{\left(\frac{1}{v_1}+\frac{1}{v_2}\right)\exp\left(\frac{E_g-qV_p+qV_a}{kT}\right)-\frac{1}{v_1}\cdot\frac{v_{D,n}}{v_{D,p}}\cdot\frac{N_CN_D}{n_i^2}\cdot\frac{E-1}{E+1}\cdot\left(1+\exp\left(\frac{qV_a}{kT}\right)\right)}\right] \tag{42}$$

Finally, the question whether the p-region is totally depleted is easily answered by comparing the values obtained from (39) and (42). If $\psi_{\rm MB} \leq \psi_C(x_1)$, then the p-region is totally depleted, whereas if $\psi_{\rm MB} > \psi_C(x_1)$, the p-region is not totally depleted.

ACKNOWLEDGMENT

The authors would like to thank the staff of the DIMES-ICP cleanrooms for their support in the fabrication of the experimental material, in particular T. L. M. Scholtes and W. de Boer. This work has been performed within a PACD project from Philips/NXP Semiconductors.

REFERENCES

[1] D. Connelly, P. Clifton, C. Faulkner, and D. E. Grupp, "Ultra-thin-body fully depleted SOI metal source/drain n-MOSFETs and ITRS low-standby-power targets through 2018," in *IEDM Tech. Dig.*, 2005, pp. 972–975.

[2] A. J. Scholten, G. D. J. Smit, M. Durand, R. van Langevelde, C. J. J. Dachs, and D. B. M. Klaassen, "A new compact model for junctions in advanced CMOS technologies," in *IEDM Tech. Dig.*, 2005, pp. 200–203.

[3] K. Matsuzawa, K. Uchida, and A. Nishiyama, "A unified simulation of Schottky and ohmic contacts," *IEEE Trans. Electron Devices*, vol. 47, no. 1, pp. 103–108, Jan. 2000.

[4] S.-D. Kim, C.-M. Park, and J. C. S. Woo, "Advanced model and analysis of series resistance for CMOS scaling into nanometer regime—Part I: Theoretical derivation," *IEEE Trans. Electron Devices*, vol. 49, no. 3, pp. 457–466, Mar. 2002.

[5] V. Venkataraman, S. Nawal, and M. J. Kumar, "Compact analytical threshold-voltage model of nanoscale fully depleted strained-Si on Silicon–Germanium-on-Insulator (SGOI) MOSFETs," *IEEE Trans. Electron Devices*, vol. 54, no. 3, pp. 554–562, Mar. 2007.

[6] E. H. Rhoderick and R. H. Williams, *Metal-Semiconductor Contacts*, 2nd ed. Oxford, U.K.: Clarendon, 1988.

[7] S. M. Sze, *Physics of Semiconductor Devices*, 2nd ed. New York: Wiley, 1981.

[8] R. T. Tung, "Recent advances in Schottky barrier concepts," *Mater. Sci. Eng., R Rep.*, vol. 35, no. 1, pp. 1–138, Nov. 2001.

[9] S.-D. Kim, C.-M. Park, and J. C. S. Woo, "Advanced source/drain engineering for box-shaped ultrashallow junction formation using laser annealing and pre-amorphization implantation in sub-100-nm SOI CMOS," *IEEE Trans. Electron Devices*, vol. 49, no. 10, pp. 1748–1754, Oct. 2002.

[10] *International Workshop on Junction Technology IWJT 2000–2008*.

[11] Q. W. Ren, "Novel contacts and diodes for advanced silicon technology," Ph.D. dissertation, ECTM, Delft Univ. Technol., Delft, The Netherlands, 2002.

[12] Q. W. Ren, L. K. Nanver, and J. W. Slotboom, "Current transport in the ultra-shallow abrupt Si and SiGe diodes," in *Proc. SAFE*, Veldhoven, The Netherlands, 2000, pp. 113–118.

[13] G. A. M. Hurkx, H. C. de Graaff, W. J. Kloosterman, and M. P. G. Knuvers, "A new analytical diode model including tunneling and avalanche breakdown," *IEEE Trans. Electron Devices*, vol. 39, no. 9, pp. 2090–2098, Sep. 1992.

[14] A. Haggag and K. Hess, "Analytical theory of semiconductor p-n junctions and the transition between depletion and quasineutral region," *IEEE Trans. Electron Devices*, vol. 47, no. 8, pp. 1624–1629, Aug. 2000.

[15] D. B. M. Klaassen, "A unified mobility model for device simulation," in *IEDM Tech. Dig.*, 1990, pp. 357–360.

[16] M. Popadić, L. K. Nanver, and T. L. M. Scholtes, "Schottky barrier height modulation by ultra-shallow low-dose dopant diffusion," in *Proc. 8th ICSICT*, Shanghai, China, 2006, pp. 469–471.

[17] M. Popadić, L. K. Nanver, and T. L. M. Scholtes, "Ultra-shallow dopant diffusion from pre-deposited RPCVD monolayers of arsenic and phosphorus," in *Proc. 15th IEEE Int. Conf. Advanced Therm. Process. Semicond. RTP*, Catania, Italy, 2007, pp. 95–100.

Miloš Popadić was born in Belgrade, Serbia, in 1981. He received the M.Sc. degree in electrical engineering from the University of Belgrade, Belgrade, in 2005. He is currently working toward the Ph.D. degree at Delft University of Technology, Delft, The Netherlands.

Since 2005, he has been with the Delft Institute of Microsystems and Nanoelectronics, Delft University of Technology, where he is involved with the electrical properties of contacts and ultrashallow junctions.

Gianpaolo Lorito was born in Salerno, Italy, in 1974. He received the degree in electronics engineering (*cum laude*) from the University of Naples Federico II, Naples, Italy, and the M.S. degree from Delft University of Technology, Delft, The Netherlands, with a thesis on the offset voltage in silicon-on-glass PNP bipolar transistors. Since 2006, he has been working toward the Ph.D. degree at the Delft Institute of Microsystems and Nanoelectronics, Delft University of Technology, where he is fully involved in the design, fabrication, and electrical characterization of silicon-on-glass SiGe HBTs for high-frequency applications.

Lis K. Nanver (S'80–M'83) received the M.Sc. degree in physics from the University of Aarhus, Aarhus, Denmark, in 1979, the Dr.Ing. degree from the Ecole Nationale Supérieure des Télécommunications, Paris, France, in 1982, where she worked on the simulation of CCD structures, and the Ph.D. degree from the Delft University of Technology, Delft, The Netherlands, in 1987, where she developed a medium-frequency BIFET process.

In 1988, she joined the IC Process Research Sector, Delft Institute for Microsystems and Nanoelectronics (DIMES), Delft University of Technology, as Bipolar Process Research Manager. She became an Associate Professor and later a Professor with the Faculty of Electrical Engineering, Mathematics and Computer Science, Delft University of Technology, detached at DIMES Technology Center in 1994 and 2001, respectively. Within the Laboratory of Electrical Components, Technology and Materials, she manages the research on the integration of silicon devices, mainly for RF, microwave, or smart sensor applications. This research involves technologies such as epitaxy by chemical-vapor or metal-induced solid-phase deposition, excimer laser processing, and substrate transfer techniques.

Prof. Nanver has served on the committees of ESSDERC, BCTM, IWJT, RTP, and SBMicro.